



Full Length Article

Soot primary particle size dependence on combustion pressure in laminar ethylene diffusion flames

Peter H. Joo, Ben Gigone, Elizabeth A. Griffin, Moah Christensen, Ömer L. Gülder*

University of Toronto Institute for Aerospace Studies, University of Toronto, 4925 Dufferin Street, Toronto, Ontario M3H 5T6, Canada

ARTICLE INFO

Keywords:

Soot size at high pressures
High-pressure soot formation
Laminar diffusion flames at pressure

ABSTRACT

A multi-probe thermophoretic soot sampling system, installed inside a high pressure combustion chamber, was used to collect soot samples at elevated pressures from ethylene–air laminar diffusion flames. Ethylene was diluted with nitrogen at a ratio of 1/3 by mass, and a constant mass flow rate of ethylene–nitrogen mixture was maintained at pressures of 5, 10, 15, and 20 bar. Selected mass flow rate of ethylene, 0.72 mg/s, provided stable and non-smoking laminar flames with a height of about 16 mm at all pressures considered. Soot samples were collected on transmission electron microscope grids at three heights above the burner rim, 3, 8, and 12 mm. The images of the soot particles were captured by transmission electron microscope and the primary soot particle diameters were determined using an automated edge detection method. The mean primary soot particle diameter increased from the sampling height of 3 mm to 8 mm, which corresponds to the mid-height of the flames where the peak soot volume fractions are observed. The soot diameters decreased from the mid-height of the flame to the sampling location of 12 mm, near the tip of the flame. The mean diameter of the primary soot particles increased with increasing pressure up to 15 bar; at 20 bar, the mean soot diameter seemed to reach a plateau or start decreasing. Measured soot volume fractions at sampling locations of 3 and 8 mm above the burner rim indicate that, in view of the measured mean soot diameters at the same locations, soot number density should be increasing intensely with pressure.

1. Introduction

Combustion engines utilized to power aircraft and land-based transportation vehicles operate at elevated pressures for reasons of improved thermodynamic efficiencies. Soot, however, is one of the undesired by-products of combustion in gas turbine and diesel engines, in which the combustion mode is mostly non-premixed, and the soot formation rate is enhanced significantly by increasing combustion pressure. Although most of the soot is oxidized within the combustion chamber of these engines, a small amount of soot escapes the oxidative process and soot particles are released into the atmosphere in the form of particulate matter (also known as smoke or black carbon) from the engine exhaust. Damaging impacts of soot emissions on climate change and the health of humans have been well-documented as well as its harmful effects in combustion devices. Efforts to find solutions for the reduction and elimination of soot particle emissions are usually held back by a lack of sufficient comprehension of soot formation and oxidation processes. Experimental and computational studies in tractable flames could help to improve our understanding of the influences of various parameters on soot processes at elevated pressures.

Recently, there has been a strong interest in experimental and numerical high pressure soot studies, mostly using gaseous fuels, focussing on the influence of pressure on soot production with the aim of identifying and assessing the prevalent mechanisms and processes [1,2]. As a result, a relatively mechanistic portrayal of soot formation at elevated pressures is emerging [2,3]. However, the utility and the use of such depictions in dealing with practical combustion systems, either in modelling efforts or interpretation of the exhaust soot measurements, have yet to be demonstrated.

Soot particle size and morphology are crucial parameters in evaluating and appraising the influence of soot on the well-being of the planet and its inhabitants. Soot aggregate characteristics are essential information in assessing the radiation forcing of atmospheric black carbon [4] as well appraising the health effects on humans [5]. For the purpose of unravelling the underpinnings of the soot processes, the temporal history of primary soot particle size and soot aggregate morphology, which carry the trails of the soot processes through the course of combustion, could be followed [6]. These footprints, which could be inferred from the experimental results obtained by following the evolution of the size and morphology of the soot particles within

* Corresponding author.

E-mail address: ogulder@utias.utoronto.ca (Ö.L. Gülder).

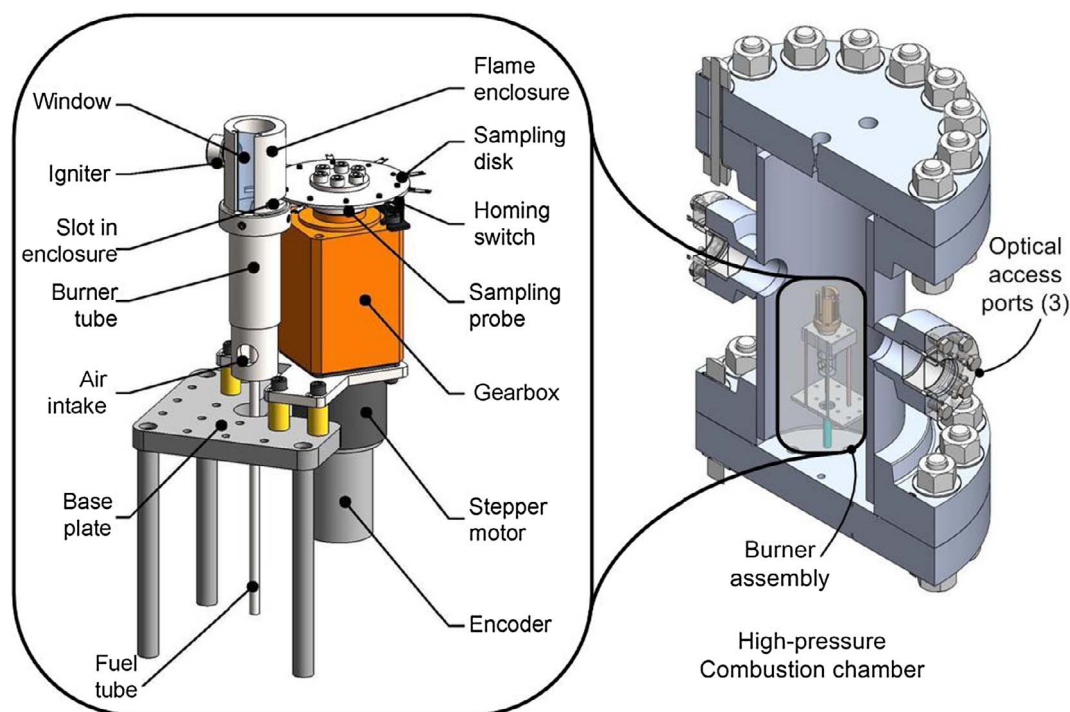


Fig. 1. Cross section of the high-pressure combustion chamber with the thermophoretic sampling system and the burner assembly. The details of the sampling system and the burner assembly are shown in the blowout view on the left.

tractable flames, can provide means to understand better the soot formation processes. While studies regarding the effects of pressure on global soot parameters (such as soot concentration) are more abundant, only a few experimental studies have been conducted on the effects of pressure on soot particle size and morphology, mainly due to difficulties in designing experimental apparatus that will sustain tractable diffusion flames and permit measurements using various diagnostic techniques [1].

To our knowledge, Flower and Bowman [7] reported first measurements of primary soot particle size in laminar diffusion flames at pressures above atmospheric using static-light scattering. Using a Wolfhard-Parker burner, they found that the mean particle size increases with pressure from atmospheric to 2.5 bar. However, it is problematic to assign the changes in soot size to pressure only, because the flames they probed were not tractable; the fuel mass flow rate was not kept constant as the pressure was increased. Kim et al. [8] reported primary soot particle size measurements by thermophoretic sampling, and subsequent analysis by electron transmission microscopy (TEM), on the centerline of diluted ethylene-oxygen laminar diffusion flames. They concluded that primary soot particle size increases with pressure in laminar diffusion flames. However, they did not keep the fuel mass flow rate constant at all pressures in their experiments. In addition, it should be noted that the fuel-oxygen diffusion flame structure is radically different than that of the flames using air as the oxidant at elevated pressures [9].

In one of the first applications of laser induced incandescence (LII) at elevated pressures, Thomson et al. [10] measured the primary soot particle size in tractable laminar methane-air flames between 5 and 40 bar. Similarly to previous two studies [8,9], they observed a steep increase in primary soot particle size from 5 to 40 bar. However, as explained by the authors [10], what is measured with LII is the effective primary soot particle size, due to the fact that the shielding effect on heat conduction between aggregated particles and the surrounding gas could not be accounted for. In a more recent work, Steinmetz et al. [11] reported primary soot particle size measurements in nitrogen diluted ethylene-air laminar diffusion flames at pressures up to 16 bar using light-extinction and scattering techniques. They found that the primary

soot particle diameters increased about 40 fold from 4 bar to 16 bar. Similar to Thomson et al. [10] results, Steinmetz et al. [11] explained that what is measured is something in between the primary soot particle size and soot aggregate size.

Soot aggregate morphological data and primary soot particles diameter measurements performed in diesel engine combustion chambers are generally affected by the parameters such as engine load, global equivalence ratio, crank angle, injection pressure, and engine speed. As a result, it is a formidable challenge to interpret the results to isolate and ascertain the effect of pressure on the soot particles because these competing parameters cannot be controlled independently [12–14].

It seems that the use of the current LII and the light scattering/extinction techniques in soot size and aggregate morphology measurements are not possible because of the challenges in quantifying the uncertainties introduced at elevated pressures. As a consequence of the present optical limitations of LII and light scattering, thermophoretic sampling and TEM analysis, although intrusive, seem to be one of the plausible methodologies for investigating the influence of pressure on the primary soot size and morphology in tractable flames [15,16]. The first thermophoretic soot sampling measurements, to the authors' knowledge, in tractable high-pressure laminar diffusion flames of methane-air were reported by Vargas and Gülder [15,16]. The mean soot primary particle size in a methane diffusion flame, measured at a constant height of 3 mm above the burner exit at all pressures, decreased about 35% from 2 to 10 bar [16].

Measurements of mean primary soot particle size, soot temperature, and soot volume fraction in nitrogen-diluted ethylene-air diffusion flames at pressures up to 20 bar were conducted and results are reported in this paper. A high pressure combustion chamber, suitable for sustaining stable and tractable laminar diffusion flames with various fuels, was modified to be fitted with a multi-probe thermophoretic soot sampling system. Soot samples collected at various pressures on TEM grids were analyzed to infer the primary soot particle size at selected heights within the flames at a pressure range from 5 to 20 bar by processing the soot aggregate images captured by TEM. The observed changes in the primary soot size are discussed considering the associated temperatures at different pressures.

2. Experimental methodology

The high pressure combustion chamber, the burner, and the thermophoretic soot sampling system for the collection of physical soot samples for this work have been previously described, see, e.g. [15–20]. Only a brief description of the experimental apparatus is provided here. A sectional cut of the high-pressure combustion chamber with the thermophoretic sampling system and the burner assembly is shown in Fig. 1.

The high pressure combustion chamber was designed to operate at pressures up to 110 bar, with an internal height and diameter of 600 and 240 mm, respectively. The optical access into the chamber is provided by three ports mounted at locations 0°, 90°, and 180° that allow line-of-sight as well as 90° scattering measurements. The burner used in this study is a circular co-flow laminar diffusion type burner. The inner diameter of the fuel tube is 3 mm and has a porous metal insert to generate a uniform velocity profile at the burner exit. The inner diameter of the co-flow air nozzle is 25 mm, and the air nozzle is also fitted with a porous metal insert to minimize the flow non-uniformities as the flow exits the nozzle.

An isometric view of the thermophoretic sampling system that was used to physically collect soot samples is depicted in Fig. 1. The sampling system consists of a circular sampling disk, a motor drive, and a programmable control system. The circular sampling disk is fitted with ten probe arms that each extend radially outwards, as shown in Fig. 2. Each probe arm has a pocket located at the end of the arm which holds a 3 mm TEM grid to collect the soot samples. Each pocket has a 2.5 mm slot that exposes the mesh of the TEM grid to the flame, and has a diameter and height of 3.3 mm and 0.5 mm, respectively. The programmable control system regulates the rotation of the sampling disk as the probe arm travels through the flame cross-section at a given height above the burner rim. After the probe arm completes sampling through the flame, the sampling disk comes to a complete stop to allow the flame to recover from disturbances caused by the probe arm. This process is repeated for the next sampling probe once the flame became stable again. The sampling time, that is the residence time of the sampling probe within the flame varied from 4 to 10 ms depending on the sampling location.

An automated image detection method was applied to the TEM

digital images. A three-stage image processing sequence was used to reduce noise in the image and perform Canny Edge detection whose details are given by Wang et al. [21].

Ethylene mass flow rate was fixed at 0.72 mg/s and the nitrogen mass flow rate was fixed at 2.16 mg/s for all the pressures considered, that is, ethylene to nitrogen dilution ratio was 1 to 3 by mass. These mass flow rates of ethylene and nitrogen provided stable and non-smoking laminar flames with a height of about 16 mm throughout the pressure range of interest. Ethylene is not a common fuel for combustion systems, but it has been used as fuel in most soot studies in laboratory flames and for empirical soot formation models. Further, ethylene is one of the most common olefins observed as an intermediate species in the diffusive combustion of larger molecule hydrocarbons. Ethylene also could be considered as a simple and gaseous surrogate for aviation kerosene, especially for soot related studies.

Soot samples on TEM grids were collected at heights of 3, 8 and 12 mm above the burner rim at pressures of 5, 10, 15, and 20 bar. Soot temperature and soot volume fraction at the same sampling locations were measured using the spectral soot emission technique whose details are given by Snelling et al. [22], therefore only a short account will be given here.

The soot spectral emission technique, which is a method utilized commonly in soot research, was used to measure the soot concentration at different points in the flames as well as to estimate the temperature profiles of the flames [1,22]. This diagnostic technique measures the radiation emitted from soot along a given chord in an axisymmetric laminar diffusion flame. Using this technique, the temperature and the soot volume fraction can be inferred without the involvement of a laser or light illumination. Information from multiple wavelengths is needed to resolve the soot concentration and temperature radially in an axisymmetric laminar diffusion flame using spectral emission. The existing spectral emission setup at this laboratory consists of a spectrometer attached to a CCD camera. The radiation from the flame is focused into the spectrometer using an adjustable aperture in front of a lens. The spectrometer produces a spectrum of the radiation which is then recorded by the CCD camera as line-of-sight emission intensity. The exposure time is based on the optimal intensity count registered on the CCD. The line-of-sight intensity data then can be inverted using an Abel-type algorithm to obtain radially resolved soot and temperature data [23,24].

3. Results and discussion

Still photographic images of the nitrogen-diluted ethylene-air diffusion flames at pressures from 1 bar to 20 bar are shown in Fig. 3. Nitrogen-diluted ethylene flames, with the fixed mass flow rate of the fuel, displayed a fully buoyancy-dominated behaviour at all pressures. The flames maintained a constant flame height for all of the pressures which is consistent with other works [25–27]. Constancy of the flame height indicates that all the species in the flame envelope have the same residence time, and thus the measurements made at the same vertical position in the flame at different pressures could be compared.

Representative transmission electron microscope images showing the soot aggregates at 8 mm above the burner at various pressures are depicted in Fig. 4. The soot particles observed in the TEM images were clustered together in small groups, but most were observed in large aggregates that were linked together in chain-like forms with many overlapping soot particles. Primary soot particle diameters evaluated from TEM images acquired at 3 sampling locations along the flame height are presented in Fig. 5 as 3 panels, one for each sampling height at 5–20 bar pressure. To show an overall picture of the primary soot diameter change with pressure and sampling location within the flame, mean primary particle sizes are plotted in Fig. 6.

The primary soot particle diameters show an increasing trend with increasing pressure at all measured locations in the flame except at 20 bar. At 12 mm vertical location in the flame there was no effective

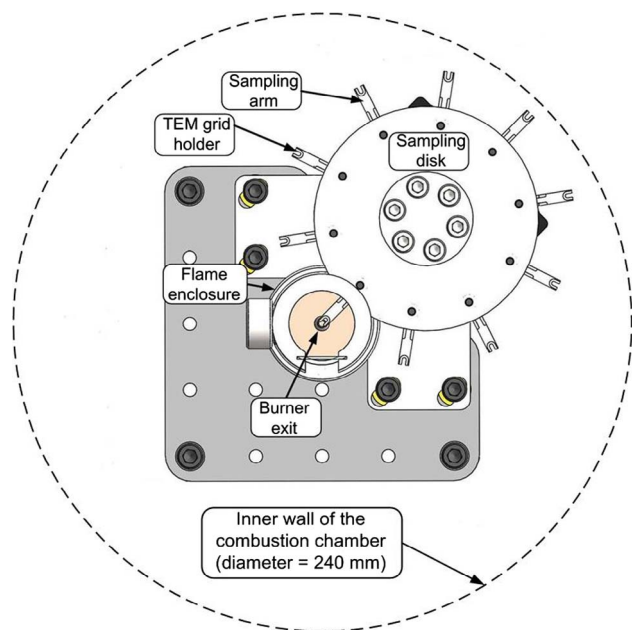


Fig. 2. Top view of the sampling system and the burner with respect to the combustion chamber inner wall. The TEM grid at the end of one of the sampling probe arms is shown concentric with the flame axis.

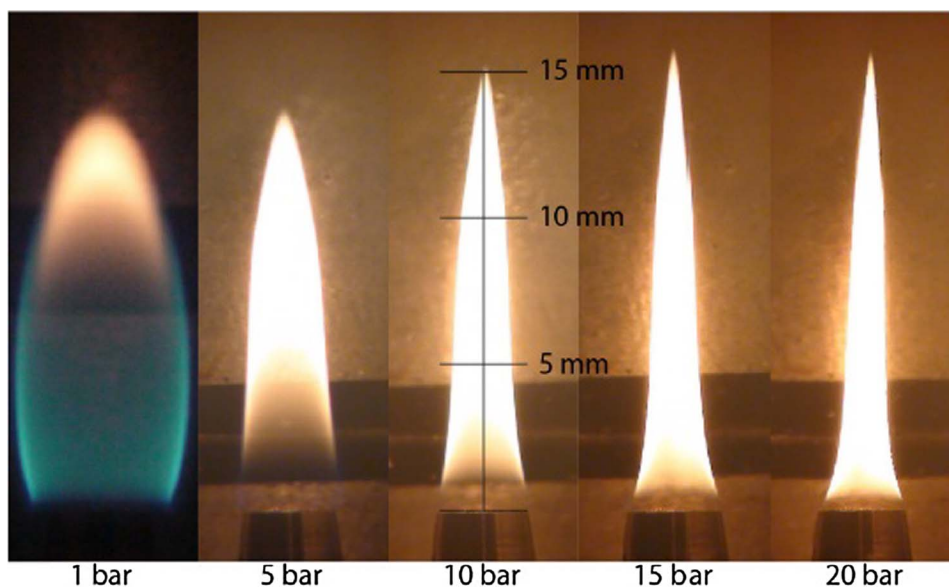


Fig. 3. Nitrogen diluted ethylene-air laminar diffusion flame from 1 to 20 bar. Nitrogen flow rate is 2.16 mg/s and ethylene flow rate is 0.72 mg/s, and kept constant at all pressures.

change in the soot particle diameters from 5 to 10 bar. The mean particle diameters at 5 and 10 bar are 33 and 32 nm, respectively. At 15 bar, however, the primary soot particle diameters increased by over 10 nm, but then at 20 bar the particle diameters decreased by about the same amount. It should be noted that at this sampling position and at elevated pressures, the flame narrows to a slender cone so any small

misalignment in the sampling system could affect the measurement significantly. However, the soot particle diameters at 12 mm position for each pressure are consistently smaller than the particles at 8 mm position. It should be noted that the axial locations from about the mid-height to the flame tip are considered as the soot oxidation dominated region in laminar diffusion flames, and at the flame tip soot

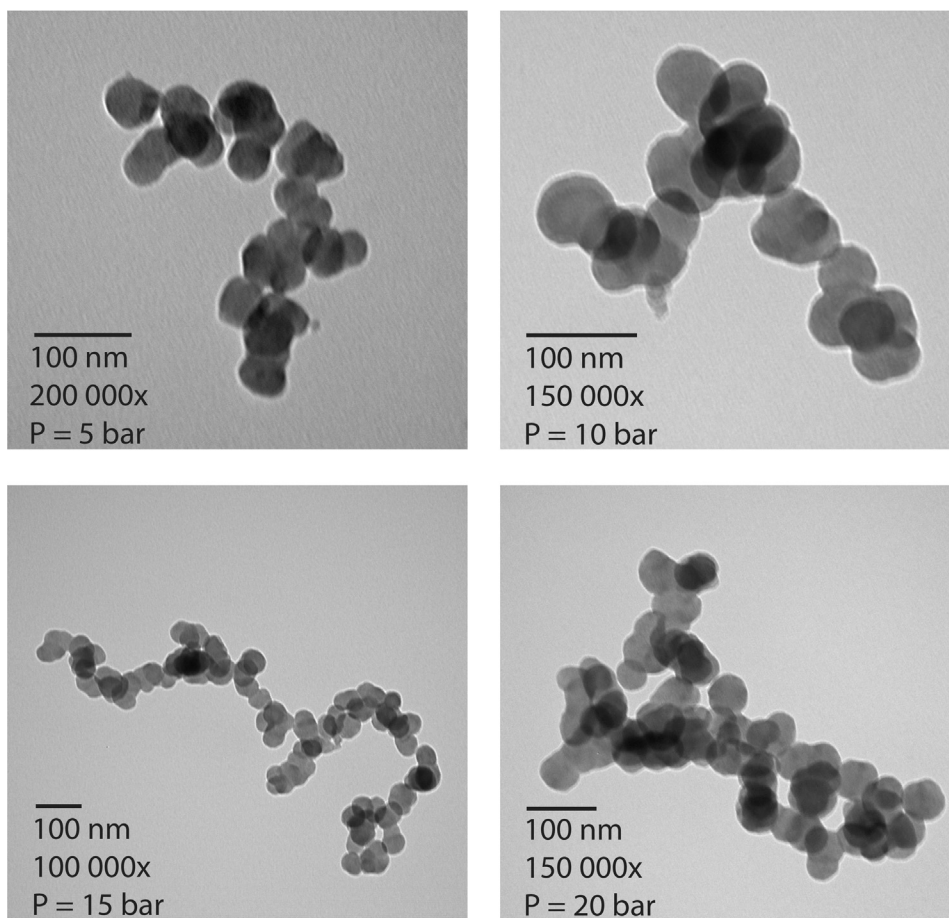


Fig. 4. Representative TEM images showing aggregated soot particles at various pressures at a height of 8 mm above the burner rim. Note that the scale bar size is not the same in all images.

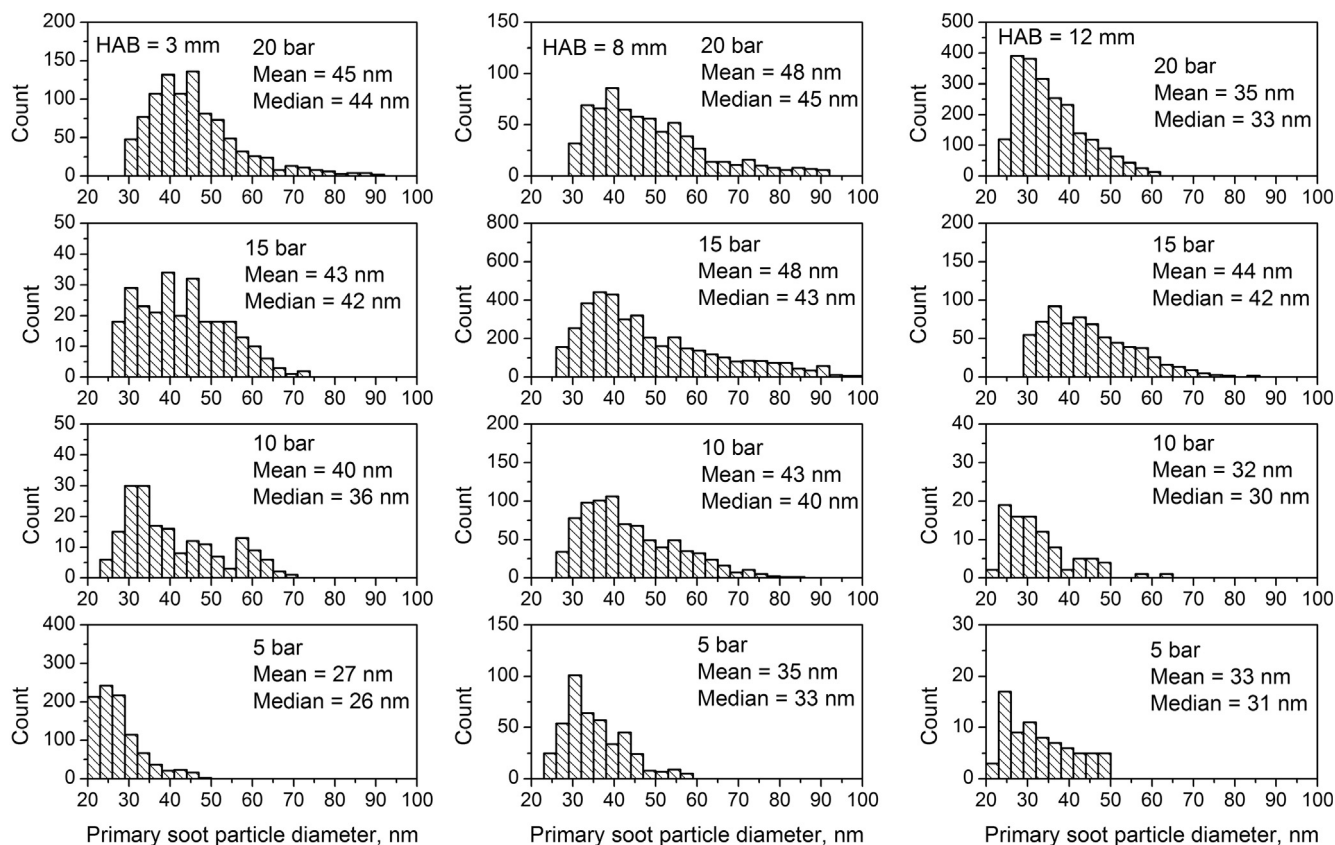


Fig. 5. Distribution of primary soot particle diameters at 3, 8 and 12 mm above the burner rim at pressures 5, 10, 15, and 20 bar. HAB = height above the burner rim.

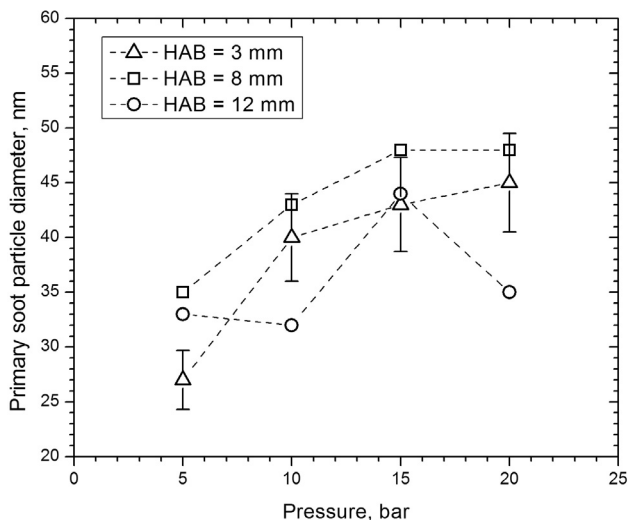


Fig. 6. Mean primary soot particle diameters at 3, 8, and 12 mm height above the burner rim at different pressures. Dashed lines are given as guides to the eye. Error bars indicate the total uncertainty.

concentration becomes zero in non-smoking flames.

Radial soot concentration and temperature profiles at 3 and 8 mm above the burner rim for all pressures considered are shown in Figs. 7 and 8, respectively. The peak soot concentrations are observed at the annulus of the flame and increased with increasing pressure. Near the mid-point of the flame, the soot concentration is the highest and the diameters of the primary soot particles are the largest, Figs. 6–8. As the soot particles are transported to higher vertical locations in the flame, surface growth of the soot particles slows down and the oxidation becomes the dominant mechanism in the upper half of the flame. Near the

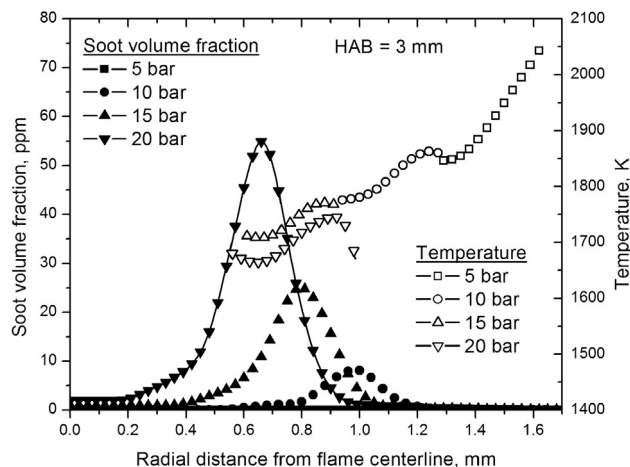


Fig. 7. Radially resolved soot volume fractions and temperatures at 3 mm at pressures 5, 10, 15, and 20 bar. Maximum soot volume fraction at 5 bar is about 0.6 ppm and it is close to the detection limit of the current measurement system.

tip of the flame, soot concentration is lower and the diameters of the primary soot particles are smaller.

Lower in the flame at 3 mm height, soot concentrations are relatively low as compared to those at 8 mm height. An increase in pressure from 5 to 20 bar resulted in a factor of about 90 increase in soot concentration while the soot temperatures decreased due to increased radiative heat loss with increasing soot concentrations, Figs. 7 and 8. The decrease in mean temperatures from 5 bar to 20 bar is about 200 K at 3 mm with similar decrease at 8 mm. In various soot modelling approaches, the rate of soot nucleation is assumed to scale with the square root of temperature, whereas it scales with the square of pressure. With increasing pressure, the soot inception rate is increased due to the

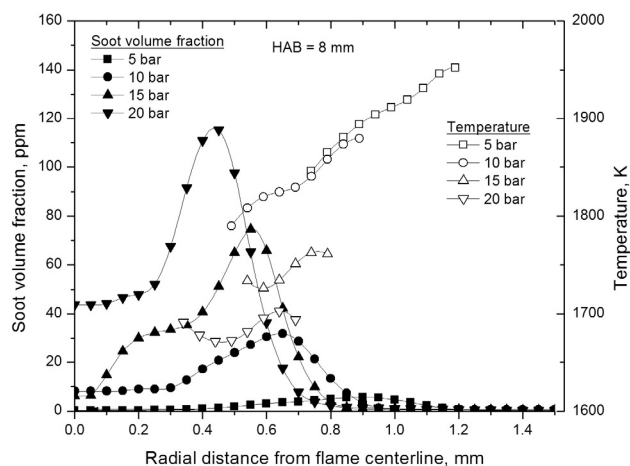


Fig. 8. Radially resolved soot volume fractions and temperatures at 8 mm at pressures 5, 10, 15, and 20 bar.

increased collision rate of PAH molecules and results in higher soot particle size and higher concentrations.

Considering the changes in soot volume fraction and primary soot particle diameter with pressure at 8 mm sampling location, it is seen that the increase in maximum soot volume fraction from 5 to 20 bar is about a factor of 50 (Fig. 8), whereas the increase in mean primary soot particle diameter is about 30% (Fig. 6) within the same pressure range. Although the soot volume fraction scales with the cube of the soot particle diameter, a very high increase in soot volume fraction can be explained only if the soot number density has a strong dependence on pressure. This means that the number of nuclei formation must have a strong sensitivity to pressure. If we assume that the soot nucleation is mainly dominated by the collision of smaller PAH molecules (such as pyrene or higher), this process yields increasing number of nuclei as the pressure increases. Coalescence of small soot particles and surface growth are believed to contribute to the final primary soot particle size. In soot surface growth, HACA is believed to be the prevailing mechanism in which the hydrogen radical plays a major role. On the other hand, hydrogen radical concentrations have shown to be decreasing with increasing pressure, via the enhanced third-body recombination reactions [27]. It is expected that this would lead to a reduced soot surface growth as the pressure increases, although Guo et al. [28], based on their numerical simulation of ethylene flames at 1–7 bar, argued that surface growth by HACA increases with pressure albeit at a very slow rate as compared to inception and PAH condensation. Observed increases in the primary soot particle size, although relatively small, in the current work with pressure could be attributed to the enhanced coalescence of smaller soot particles.

It should be mentioned here that the rate of coalescence might depend on the Knudsen number, defined as the ratio of the mean free path of the gas to the diameter of the soot particle, which would be changing as the pressure increases. If the size of the small soot particles, which go through coalescence, is in the order of few nanometers, then the Knudsen number would change from about 50 to 10 for going from 5 to 20 bar for a 2 nm particle. For a particle of 10 nm, the Knudsen number range would be about from 10 to 2. These Knudsen numbers are within the transition regime [29]. In molecular and continuum regimes, coalescence rate of particles can be formulated using basic theoretical principles; however, in the transition regime, usually depicted as $1 < Kn < 10$, the practice is to use the Fuchs coagulation kernel or harmonic mean of the free-molecular and slip-flow regimes kernels, see e.g. [30]. In their formulation of the harmonic mean coagulation kernel and subsequent analysis, Park et al. [29] show that coagulation rate increases from Kn number 40 to about 5 where it changes direction and decrease with decreasing Kn number.

The experimental results of Flower and Bowman [7] with pure

ethylene diffusion flames indicated that the primary soot particle diameters and soot number density increase with pressure and with height along the flame centerline. They attributed these observations to increased surface growth and particle nucleation rates with increasing pressure. Current results cannot be compared to those of Flower and Bowman [7] because of their experimental protocol that permitted the fuel mass flow rate be increased linearly with pressure. Then, the growth of the particles and the increase in the soot number density are not only affected by the pressure, but also from the increased supply of fuel molecules. As discussed in the Introduction briefly, the measurements of Kim et al. [8] suffers from the same deficiency that the mass flow rate of the fuel was not kept constant, but increased, as the pressure went up.

Although the experiments of Thomson et al. [10] and Steinmetz et al. [11] were conducted on tractable laminar diffusion flames with fixed fuel mass flow rates, their measurements suffer from the inadequacy of the optical techniques used at elevated pressures. As recognized by the authors of both studies [10,11], what is measured is most probably an intermediate size between primary soot diameter and the soot aggregate size. Therefore it is not possible to know if the increase in the particle diameter measurements is caused by pressure, aggregate characteristics, or both.

Vargas and Gülder [16] reported measurements of primary soot particle diameters in methane diffusion flames at 3 mm above the burner rim at various pressures. The fuel flow rate was lower than the current fuel rate and the resulting flames were about 10 mm long at pressures from 2 to 10 bar. At 3 mm sampling location, the mean primary soot diameter decreased steadily with increasing pressure from 2 to 10 bar. This contradicts the current findings that at 3 mm above the burner rim, the mean primary soot particle diameter increases with pressure in ethylene diffusion flames. This apparent disagreement points to the non-trivial dependence of soot formation and growth processes on fuel chemistry, mass flow rate of the fuel, dilution rate, and pressure in laminar diffusion flames.

It was shown that, at atmospheric conditions, the primary soot particle sizes could differ from the flame wings to the flame centerline [31]. However, using the current experimental setup it is not possible to resolve the primary soot size radially. The diameters of the cross sections of the flames at sampling locations at 5 bar are smaller than 3 mm, and they decrease with increasing pressure, Fig. 3. Due to restraints imposed by the size of the TEM sampling grids and the diameter of the laminar diffusion flames at elevated pressures, the primary soot diameter data reported here represent diameters averaged over the flame cross-sectional area at the sampling height above the burner rim.

It is a challenging task to evaluate potential influences of the variables such as particle number density, soot aggregate size, temperature at the sampling location, and the Knudsen number on sampling and their contribution to the total uncertainty involved in the sampling process. Potential dependence of the thermophoretic force, and velocity, on Knudsen number, Kn, could lead to preferential sampling because of the change in Kn number with changing pressure and different average sizes of the soot aggregates. Assuming an average gas temperature of about 1500 K at the sampling location, the Kn number of the soot aggregates would be changing from 0.85 to 0.2 when the pressure is increased from 5 to 20 bar, for a soot aggregate size of about 100 nm. For a typical soot aggregate size of 200 nm, the Kn number would vary from 0.42 to 0.1 for the same pressure range. These Kn numbers are almost in the continuum regime, and it could be assumed that for large enough soot aggregates, the sampling would not be biased by the Kn number change at pressures of interest, to a first approximation [32]. Other potential uncertainties introduced by the physical intrusion of the sampling probe into the flame are discussed in detail in [15,16].

The experimental uncertainty in evaluating the primary soot particle diameters was estimated to be within 15% with confidence interval of 95%. This uncertainty is similar to previous measurements of the primary soot particle size by TEM imaging [33].

4. Conclusions

Due to the limited capability of existing optical techniques in measuring the primary soot particle size at pressures above atmospheric, soot aggregates from laminar nitrogen diluted ethylene-air diffusion flames were collected by thermophoretic sampling at pressures up to 20 bar. The samples were collected on transmission electron microscope grids at several axial locations within the flames and the images were captured using the transmission electron microscope. The images were processed using an automated edge detection method and the primary soot particle diameters were determined for the purpose of assessing the dependence of primary soot particle diameter on pressure. At the same sampling locations, the temperatures and soot volume fractions were measured by using the spectral soot emission technique. At mid-heights of the flames, it was found that the increase in maximum soot volume fraction from 5 to 20 bar is a factor of about 50, whereas the increase in mean primary soot particle diameter is about 30% within the same pressure range. It was argued that to achieve drastic increases in soot volume fractions with pressure, the number of soot nuclei generated must be increasing with increasing pressure in view of the observed changes in primary soot particle diameter with pressure. Dependence of soot nuclei formation and coalescence of small soot particles on pressure is discussed in relation to the Knudsen number. It can be concluded that the observed behavior of the primary soot particle size with pressure is a manifestation of enhanced coalescence of smaller soot particles with increasing pressure (decreasing Knudsen number in the range 20 to 5) in spite of the suspected reduction in surface growth by HACA mechanism. The increase in the soot volume fraction with pressure seems to be mainly dominated by the increased particle number density as the pressure is increased.

Acknowledgements

The authors thank the Natural Sciences and Engineering Research Council of Canada for a discovery grant (RGPIN-2017-06063) and the Ontario Research Fund for a Research Excellence Program grant (ORF RE07-034), awarded to the senior author, for the support of this research work.

References

- [1] Karatas AE, Gülder ÖL. Soot formation in high-pressure laminar diffusion flames. *Prog Energy Combust Sci* 2012;38:818–45.
- [2] Abdelgadir A, Rakha IA, Steinmetz SA, Atilli A, Bisetti F, Roberts WL. Effects of hydrodynamics and mixing on soot formation and growth in laminar coflow diffusion flames at elevated pressures. *Combust Flame* 2017;181: 39–33.
- [3] Gülder ÖL, Intasopa G, Joo HI, Mandatori PM, Bento DS, Vaillancourt ME. Unified behaviour of maximum soot yields of methane, ethane and propane laminar diffusion flames at high pressures. *Combust Flame* 2011;158:2037–44.
- [4] Bond TC, Doherty SJ, Fahey DW, et al. Bounding the role of black carbon in the climate system: a scientific assessment. *J Geophys Res Atmos* 2013;118:5380–552.
- [5] Jannsen NAH, Hoek J, Milena S-L, et al. Black carbon as an additional indicator of the adverse health effects of airborne particles compared with PM10 and PM2.5. *Environ Health Perspect* 2011;119:1691–9.
- [6] Lapuerta M, Martos EJ, Herreros JM. Effect of engine operating conditions on the size of primary particles composing diesel soot agglomerates. *J Aerosol Sci* 2007;38:455–66.
- [7] Flower WL, Bowman CT. Measurements of the structure of sooting laminar diffusion flames at elevated pressures. *Proc Combust Inst* 1984;20:1035–44.
- [8] Kim CH, Xu F, Faeth GM. Soot surface growth and oxidation at pressures up to 8.0 atm in laminar nonpremixed and partially premixed flames. *Combust Flame* 2008;152:301–16.
- [9] Joo PH, Charest MR, Groth CPT, Gülder ÖL. Comparison of structures of laminar methane-oxygen and methane-air diffusion flames from atmospheric to 60 atm. *Combust Flame* 2013;160:1990–8.
- [10] Thomson K, Snelling DR, Smallwood GJ, Liu F. Laser induced incandescence measurements of soot volume fraction and effective particle size in a laminar co-annular non-premixed methane/air flame at pressures between 0.5–4.0 MPa. *Appl Phys B* 2006;83:469–75.
- [11] Steinmetz SA, Fang T, Roberts WL. Soot particle size measurements in ethylene diffusion flames at elevated pressures. *Combust Flame* 2016;169:85–93.
- [12] Lee KO, Cole R, Sekar R, Choi MY, Kang JS, Bae CS, et al. Morphological investigation of the microstructure, dimensions, and fractal geometry of diesel particulates. *Proc Combust Inst* 2002;29:647–53.
- [13] Leidenberger U, Mühlbauer W, Lorenz S, Lehman S, Brüggemann D. Experimental studies on the influence of Diesel engine operating parameters on properties of emitted soot particles. *Combust Sci Technol* 2012;184:1–15.
- [14] Mathis U, Mohr M, Kaegi R. Influence of diesel engine combustion parameters on primary soot particle diameter. *Environ Sci Technol* 2005;39:1887–92.
- [15] Vargas AM, Gülder ÖL. A multi-probe thermophoretic soot sampling system for high-pressure diffusion flames. *Rev Sci Instrum* 2016;87:055101.
- [16] Vargas AM, Gülder ÖL. Pressure dependence of primary soot particle size determined using thermophoretic sampling in laminar methane-air diffusion flames. *Proc Combust Inst* 2017;36:975–84.
- [17] Thomson KA, Gülder ÖL, Weckman EJ, Fraser RA, Smallwood GJ, Snelling DR. Soot concentration and temperature measurements in co-annular, nonpremixed CH₄/air laminar flames at pressures up to 4 MPa. *Combust Flame* 2005;140:222–32.
- [18] Bento DS, Thomson KA, Gülder ÖL. Soot formation and temperature field structure in laminar propane-air diffusion flames at elevated pressures. *Combust Flame* 2006;145:765–78.
- [19] Joo HI, Gülder ÖL. Soot formation and temperature field structure in co-flow laminar methane-air diffusion flames at pressures from 10 to 60 atm. *Proc Combust Inst* 2009;32:769–75.
- [20] Mandatori PM, Gülder ÖL. Soot formation in laminar ethane diffusion flames at pressures from 0.2 to 3.3 MPa. *Proc Combust Inst* 2011;33:577–84.
- [21] Wang C, Chan QN, Kook S, Zhan R, Kook S, Hawkes ER, et al. Automated determination of size and morphology information from soot transmission electron microscope (TEM)-generated images. *J Nanopart Res* 2016;18:127.
- [22] Snelling DR, Thomson KA, Smallwood GJ, Gülder ÖL, Weckman EJ, Fraser RA. Spectrally resolved measurement of flame radiation to determine soot temperature and concentration. *AIAA J* 2002;40:1789–95.
- [23] Dasch CJ. One-dimensional tomography: a comparison of Abel, onion-peeling, and filtered backprojection methods. *Appl Optics* 1992;31:1146–52.
- [24] Dribinski V, Ossadtchi A, Mandelshtam VA, Reisler H. Reconstruction of Abel-transformable images: the Gaussian basis-set expansion Abel transform method. *Rev Sci Instrum* 2002;73(7):2634.
- [25] Joo HI, Gülder ÖL. Experimental study of soot and temperature field structure of laminar co-flow ethylene-air diffusion flames with nitrogen dilution at elevated pressures. *Combust Flame* 2011;158:416–22.
- [26] Karatas AE, Gülder ÖL. Effects of carbon dioxide and nitrogen addition on soot processes in laminar diffusion flames of ethylene-air at high pressures. *Fuel* 2017;200:76–80.
- [27] Liu F, Karatas AE, Gülder ÖL, Gu M. Numerical and experimental study of the influence of CO₂ and N₂ dilution on soot formation in laminar coflow C₂H₄/air diffusion flames at pressures between 5 and 20 atm. *Combust Flame* 2015;162:2231–47.
- [28] Guo H, Gu Z, Thomson KA, Smallwood GJ, Baksh F. Soot formation in a laminar ethylene/air diffusion flame at pressures from 1 to 8 atm. *Proc Combust Inst* 2013;34:1795–802.
- [29] Park SH, Lee KW, Otto E, Fissan H. The log-normal size distribution theory of Brownian aerosol coagulation for the entire particle range: Part I – Analytical solution using the harmonic mean coagulation kernel. *J Aerosol Sci* 1999;30:3–16.
- [30] Patterson RIA, Singh J, Balthasar M, Kraft M, Wagner W. Extending stochastic soot simulation to higher pressures. *Combust Flame* 2006;145:638–42.
- [31] Kholghy M, Saffaripour M, Yip C, Thomson MJ. The evolution of soot morphology in a laminar coflow diffusion flame of a surrogate for Jet A-1. *Combust Flame* 2013;160:2119–30.
- [32] Talbot L, Cheng RK, Schefer RW, Willis DR. Thermophoresis of particles in a heated boundary layer. *J Fluid Mech* 1980;101:737–58.
- [33] Hu B, Yang B, Köylü ÜÖ. Soot measurements at the axis of an ethylene/air non-premixed turbulent jet flame. *Combust Flame* 2003;134:93–106.